Fluid Phase Equilibria 318 (2012) 19–24

Contents lists available at SciVerse ScienceDirect

Fluid Phase Equilibria

journal homepage: www.elsevier.com/locate/fluid

Confining effect of carbon-nanotube configuration on phase behavior of hard-sphere fluid

Huan Cong Huang[a], Jayant K. Singh[b], Jong-Min Lee[a], Sang Kyu Kwak[a,*]

[a] Division of Chemical and Biomolecular Engineering, School of Chemical and Biomedical Engineering, Nanyang Technological University, Singapore 637459, Singapore
[b] Department of Chemical Engineering, Indian Institute of Technology Kanpur, Kanpur 208016, India

ARTICLE INFO

Article history:
Received 7 June 2011
Received in revised form
30 November 2011
Accepted 22 December 2011
Available online 17 January 2012

Keywords:
Confined hard-sphere fluids
Carbon nanotube
Phase transition
Molecular dynamics

ABSTRACT

We capture the effects of the structured surface on a phase transition of hard-sphere fluids. The confining environment follows single-walled carbon nanotube (SWCNT) configuration. For careful discrimination of the surface-chirality effect, hard-core potentials are applied to carbon atoms, and further their positions are fixed. In this way, equation of states and microstructures of the confined particles are intrinsically obtained based on the SWCNT chirality as well as the diameter. We observed three branches indicating fluid-like and solid-like phases with onsets of freezing and melting. We found that freezing and melting of fluid particles are very sensitive to the surface chirality in small-diameter SWCNT, which especially holds a single layer of fluid particles. In those SWCNTs, spreading pressures are found to be lower than those of smooth-surface cylindrical pores. The surface chirality has less impact on the phase change of confined fluids for large-diameter SWCNT, of which diameter is a dominant factor.

1. Introduction

Single-walled carbon nanotubes (SWCNTs) have become one of the most potential materials in many applications such as gas storages [1–3], semi-conductors, and fabrication of nanodevices [4–7] since their discovery [8], due to their promising electrical, mechanical, and structural properties. SWCNTs are graphite sheets rolled up into cylindrical shape containing a hollow interior that can be served as a vessel for encapsulating molecules. Such characteristic has received increasing attention in recent years [9–23], but behaviors and properties of inserted particles in such a small structured-pore have not been put into a good scientific treatment. We aim to obtain them from fundamental basis by resorting to atomistic scale approach using molecular dynamics (MD) method.

Fluids confined in pores having several atom sizes exhibit significantly different properties compared to bulk under same thermodynamic conditions. Recent studies have shown that behaviors of confined fluids depend not only on interactions between the particles and the confining wall [24–29], but also on confining geometry [30–34]. In systems with soft potentials, thermodynamic properties are often the results from energetic competition of these two factors, which are not readily distinguishable except for the system with a small size pore. The tight geometrical confinement exerts a dominant effect due to suppression of interaction potentials. In this regards, hard-sphere fluids confined in hard walls have been extensively studied with respect to the pore size, which brings complex cross-over phenomena of equations of states into the phase diagram.

In this study, we carry the study of the pore size a step further by adopting forged surface composed of hard-sphere particles, of which positions follow the SWCNT configuration. Many studies have been conducted to investigate the absorption of gas molecules in CNTs both in experiments [35–37] and simulations [3,35,36] considering interaction strengths (i.e. carbon– carbon, carbon–fluid particles, fluid particles–fluid particles), radius, and chirality. However, phase behavior of freezing and melting is little explored. In particular, the question of how the surface structure affects the onset of freezing and melting, if any, is not convincingly addressed. We answer this essential question by considering the pore size and the surface chirality of SWCNT and obtaining their effects on confined hard-sphere fluids.

2. Simulation approach

The fluid particles are first arranged with cylindrically layered structures. The number of layers and the initial structure of each layer are determined with respect to the diameter of SWCNT. We used the packing method of fluid particles [34,38] by rolling-up a hexagonal plane into a cylindrical shape. The full hexagonal plane of fluid particles is made by positioning particles to centers of each hexagon of the 2D honeycomb lattice of the chosen SWCNT, and then the hexagonal plane is rolled up along with a specific

* Corresponding author.
E-mail address: skkwak@ntu.edu.sg (S.K. Kwak).

0378-3812/$ – see front matter © 2012 Elsevier B.V. All rights reserved.
doi:10.1016/j.fluid.2011.12.028

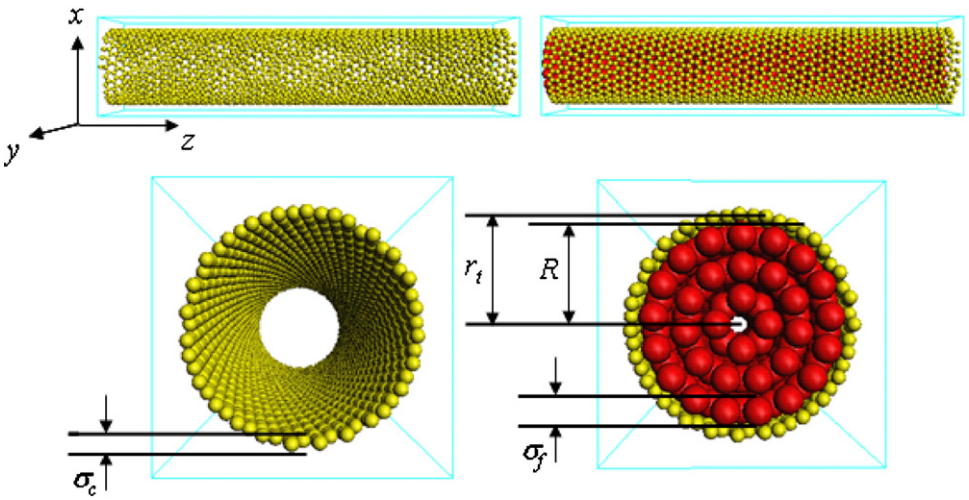

Fig. 1. Simulation screenshots of the SWCNT with chiral index (20, 3) (left); the SWCNT filled with fluid particles (red spheres) (right). (For interpretation of the references to color in this figure legend, the reader is referred to the web version of the article.)

chiral vector. The detailed procedure is as follows; (1) calculating the diameter d_t of the interested SWCNT with chiral index (n, m) and its lattice parameter a, (2) calculating the chiral index (n', m') for the hexagonal plane formed by the fluid particles. It can have the maximum diameter d_{max} less than $d_t - (\sigma_c + \sigma_f)$ where σ_c and σ_f are diameters of carbon atom and fluid particle, respectively, and the first layer of fluid particles is rolled up into a cylindrical shape with the chiral index (n', m'). The lattice parameter is chosen small enough so that fluid particles are accommodated in a high density without overlaps of fluid particles, (3) Repeating step (2) with the diameter of the cylindrical layer calculated by $d_{max} - \sigma_f$, where d_{max} is the diameter of the outer layer, and finally (4) the particles will be packed into axial layers of triangle or square, or linear zigzag structure, depending on the diameter of that layer, if the inner most layer cannot hold a rolled-up hexagonal plane (see Fig. 1). Periodic boundary condition is applied to the axial (i.e. z-axis) direction. The effective volume of SWCNT is defined as,

$$V = \pi R^2 L \tag{1}$$

where $R = r_t - 0.5\sigma_c$ is the effective radius of SWCNT (i.e. distance from core axis to inner surface of SWCNT), r_t is the radius of SWCNT (i.e. distance from core axis to the center of carbon atom), and L the length of SWCNT. We use Eq. (1) to obtain the reduced density (i.e. $\rho^* = N_f\sigma_f^3/V$) even though the actual accessible volume of SWCNT is slightly larger. Note that this discrepancy affects little to determine freezing and melting points of larger fluid particles.

We use collision-based MD method [39] to obtain the equation of states as well as axial and radial distribution functions. MD allows us to have the pressure tensor, which is calculated by the virial theorem, for the fluids confined in SWCNT. To realize the accurate onset of freezing, a sensitive method was required to monitor a subtle change in the phase of confined fluids. To do so, we apply the 2D hexagonal order parameter Φ_6 for each layer of the fluid particles and it is defined as,

$$\Phi_6 = \left| \frac{1}{M} \sum_{i=1}^{M} \frac{1}{N_i} \sum_{j=1}^{N_i} \exp(i6\theta_{ij}) \right| \tag{2}$$

where M is the number of particles in a cylindrical layer, N_i is the number of nearest neighbors of particles i. We define the nearest neighbors with particles j within a distance $1.3\sigma_f$ from particle i, and θ_{ij} is the angle between two neighboring particles i and j. The value of Φ_6 equals to 1.0 for a perfect hexagonal plane, but decreases from 1.0 for disordered phases. To calculate Φ_6, the cylindrical layers of fluid particles are unrolled into flat planes. Note that the distance of a cylindrical layer to the central axis of pore is r_0 and the cylindrical coordinate of a particle on the layer is (r, φ, z). The coordinates of all particles at the cylindrical layer are first projected to the cylinder of radius r_0, the arc length $r_0\varphi$ of the projection becomes the x coordinate and the z coordinate becomes the y coordinate on the 2D flat plane after unrolling. Periodic boundary conditions are applied to both x and y directions when the 2D hexagonal order parameter is calculated.

The fluid–fluid interaction is represented by the hard-core potential that has pure repulsive interaction,

$$u_{f-f} = \begin{cases} \infty, & r_{ij} < \sigma_f \\ 0, & r_{ij} \geq \sigma_f \end{cases} \tag{3}$$

where r_{ij} is the distance between a pair of fluid particles. The interaction between the fluid particle and carbon atom is also represented as the hard-core potential,

$$u_{f-w} = \begin{cases} \infty, & r_{ij} < 1/2(\sigma_f + \sigma_c) \\ 0, & r_{ij} \geq 1/2(\sigma_f + \sigma_c) \end{cases} \tag{4}$$

The carbon atoms are kept stationary at their lattice sites thus the momentum at collision between fluid particle and carbon atom is fully transferred back to the fluid particle. For the system under our consideration, we pay careful attention to choose it with larger size of fluid particle because the surface-chirality effect would be harder to catch. It seems contradictory, yet this particular system has shown subtle difference in the surface-chirality effect and this would be a reference indication for easier study for the system of carbon atom in larger size. In this regards, diameters of carbon atom and fluid particle are chosen to be $0.5\sigma_f$ and $1.0\sigma_f$, respectively, and the lattice parameter a is set to $0.875\sigma_f$ for SWCNT to ensure that the fluid particles do not transversely pass through SWCNT. The MD simulations are performed with the canonical ensemble (i.e. NVT – constant volume). The number of fluid particles is determined by the target density and the number of unit cells, with the equation $N = \rho V = 1/2n\rho\pi R^2|\mathbf{T}|$, where n is the number of unit cells, $|\mathbf{T}|$ is the length of a unit cell and $\mathbf{T}$ is the transitional vector of a 2D unit cell. All length scales are in unit of the diameter of fluid particle σ_f, which is taken as unity. All units are in their reduced forms if not specified. The reduced time step $\Delta t^* = \Delta t/[\sigma_f(m/kT)^{0.5}]$ is fixed at 0.05,where m is the mass of fluid particles, k is the Boltzmann factor and T is the temperature. The reduced pressure P^* is defined as $P^* = \beta P\sigma_f{}^3$, where $\beta = 1/kT$ is the inversed temperature. The momenta of all fluid particles are rescaled to satisfy the target temperature at the

Table 1
Structure parameters for the small SWCNTs.[a]

Chiral Index	Diameter ($2 \times r_t$)	Number of Carbon atoms in unit cell	Length of unit cell	Number of unit cell	Length of SWCNT	Number of carbon atoms
(6, 5)	2.6569	364	14.4573	3	43.3719	1092
(7, 4)	2.6859	124	4.87179	10	48.7197	1240
(9, 1)	2.6569	364	14.4573	3	43.3719	1091
(8, 4)	2.9475	112	4.0097	12	48.1164	1344
(9, 3)	3.0126	156	5.4643	8	43.7144	1248
(10, 1)	2.9344	148	5.3224	8	42.5792	1184

[a] All length units are reduced by the diameter of hard-sphere fluid particle, σ_f.

end of each time step under *NVT* ensemble MD simulation. The equilibration time step is set to 10^5, and then the system is switched to the microcanonical ensemble (i.e. *NVE* – constant energy) for another 2×10^5 steps for the production cycle. Three independent runs were performed to present average data.

3. Results and discussion

3.1. Small SWCNTs

First, we discuss SWCNTs, which contain one cylindrical layer of fluid particles. The chiral indices are chosen to be (6, 5), (7, 4), and (9, 1), which can hold the triangular packing (i.e. from *z*-axis basis) of fluid particles, and (8, 4), (9, 3), and (10, 1), which can hold the square packing (i.e. from *z*-axis basis) of fluid particles. The detailed parameters for these SWCNTs are listed in Table 1. It is worthy of notice that the indices are chosen to have similar diameters. The equation of states of the hard-spheres confined in the SWCNTs of indices (6, 5), (7, 4) and (9, 1) are shown in Fig. 2. Three branches of fluid-like, solid-like and coexistence are observed for all three cases. The spreading pressures are close to each other at fluid-like and solid-like densities but show considerable deviations over the density region of phase change. Interestingly, the freezing pressures of (9, 1) are a little larger compared to those of (6, 5) even though they have same diameters. This is a clear indication of the surface-chirality effect illustrating that the SWCNT (9, 1) confines fluid particles slightly more. When the cylindrical hard-wall with the same diameter (i.e. 2.1569) as in the cases of (6, 5) and (9, 1) were investigated, the spreading pressures did not show the onset of the freezing (i.e. this result is consistent with earlier work [34] as a threshold diameter to observe the onset of the freezing should be larger than ~2.16). It clearly exemplifies that the surface modification causes the phase transition. Further, dramatic suppression of the spreading pressure happens for the case of (7, 4) when the diameter is larger than 2.16 due to the surface modification. The equation of states of the hard-spheres confined in the SWCNTs of indices (8, 4), (9, 3), and (10, 1) are shown in Fig. 3, where larger deviation on the freezing behavior is found between the SWCNTs of different indices though these SWCNTs have little difference in diameter. The gradual shifts of freezing pressure and densities are observed in the order of (9, 3), (8, 4), and (10, 1). The freezing pressure of (10, 1), which is around 16, is much larger than those of other two indices. Large suppression of the spreading pressure was also found in these indices due to presence of the surface particles, but the smallest suppression is observed when the diameter is largest. In comparison of surface-chirality and diameter effects, the latter has been more clearly shown over these particular indices. Nevertheless, the results show that the structured wall of SWCNTs induces early (i.e. lower density) onset of freezing at dramatically lower pressure.

The normalized radial density profiles of the hard-spheres confined in the SWCNT (6, 5) at different average densities are shown in Fig. 4. All profiles show that the maximum local density appears near the SWCNT inner surface at the distance $r = r_t - 0.5(\sigma_c + \sigma_f)$ while the minimum value is found in the core axis of the SWCNT. The local density then decreases since the regime $r > r_t - 0.5(\sigma_c + \sigma_f)$ becomes less accessible for fluid particles. The maximum normalized local density near the inner wall of SWCNTs increases

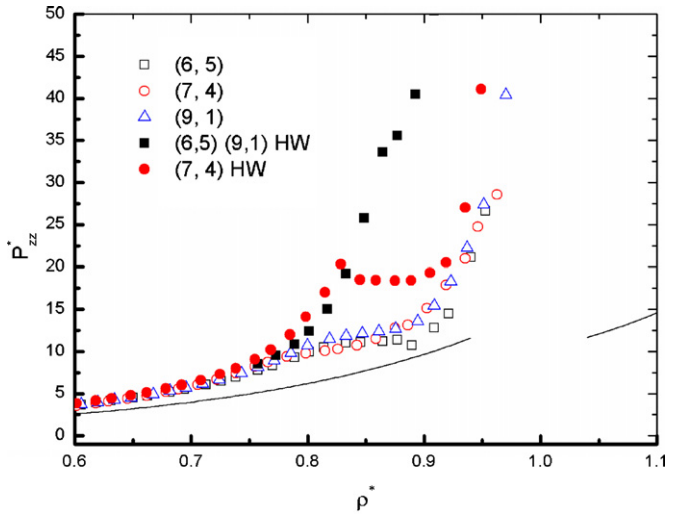

Fig. 2. The equation of states (i.e. reduced spreading pressure vs. reduced density) of hard-spheres confined in SWCNTs of chiral indices of (6, 5), (7, 4) and (9, 1), which are depicted by open symbols. The results of smooth cylindrical hard walls (HW) are depicted with filled symbols and corresponding index of SWCNT, which has a same diameter, is indicated. The line is for hard-sphere systems in bulk.

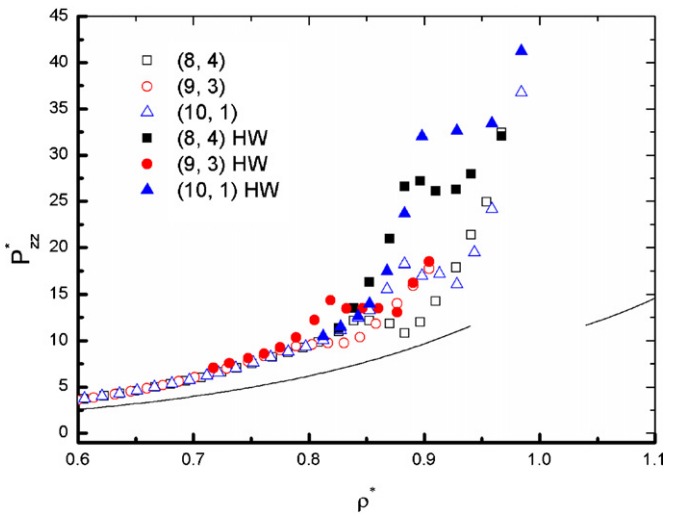

Fig. 3. The equation of states (i.e. reduced spreading pressure vs. reduced density) of hard-spheres confined in SWCNTs of chiral indices of (8, 4), (9, 3) and (10, 1), which are depicted by open symbols. The results of smooth cylindrical hard walls (HW) are depicted with filled symbols and corresponding index of SWCNT, which has a same diameter, is indicated. The line is for hard-sphere systems in bulk.

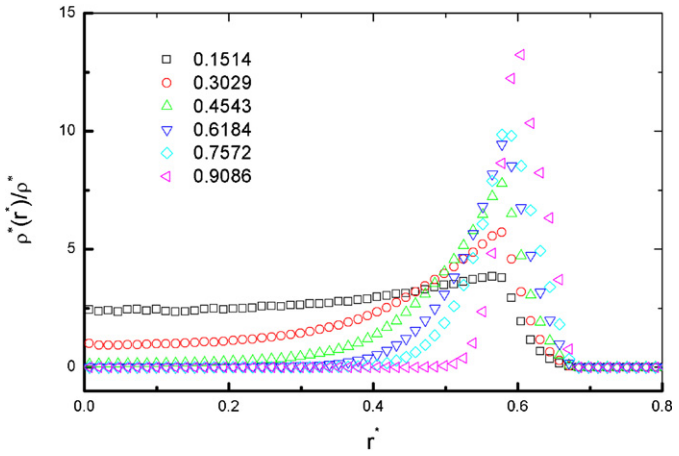

Fig. 4. Plot of normalized radial density with respect to average density of the system vs. reduced radius for hard-spheres confined in SWCNT of chiral index (6, 5) at different average densities.

with the average density, however the normalized local density near the core axis significantly decreases with the increase of the average density. For $\rho^* = 0.1514$, the normalized local density at $r^* = 0$ has the value of 2.40(3), which decreases to 0.0044(5) for $\rho^* = 0.6184$. The normalized local densities are zero at the pore axis for the average density larger than 0.6625. This behavior is similar to that of hard spheres confined in smooth cylindrical hard wall of the same diameter, where triangular packing (i.e. from z-axis basis) is clearly observable.

The axial distribution functions $g^*(z)$ for the hard-spheres confined in the SWCNT (6, 5) is shown in Fig. 5. At low densities 0.3028, 0.4543 and 0.6184 we observe similar axial distribution with the hard cylindrical pores of the same diameter. The $g^*(z)$'s have the peak value at $z = 1.0$ and decay to 1.0 at the axial distance $z > 3.0$. The fluids at these average densities are considered very short-ranged order. For large densities 0.6941, 0.7698, and 0.8140, two distinct peaks are spread to be multiple with larger values of $g^*(z)$'s, which correspond to the possible short-ranged order at the axial distance $z < 5.0$, although the system is still in the fluid-like phase. In this case, the fluid particles form tetrahedral clusters in the SWCNT. For larger densities of our interest (i.e. 0.8644, 0.8771, 0.8897, 0.9086, and 0.9212), strongly ordered-structure is observed. The $g^*(z)$'s show repeating peaks at regular interval and the peaks become sharper as the average density increases. Note that for average densities 0.8644 and 0.8771 the value of $g^*(z)$ between the peaks are not zero. The phenomenon implies a packed helical shape of fluid particles and this may be treated as a characteristic structure to have the coexistence of fluid-like and solid-like phases evident from that the pressures at these two densities are almost same. For determining the onset density of freezing and melting, a further analysis is done with the 2D hexagonal order parameter Φ_6. The result is shown in Fig. 6 for the same SWCNT where Φ_6 increases slightly with respect to average density at the fluid branch indicating slight increase of short-ranged order in the system. Φ_6 increases sharply at the onset of the freezing at $\rho^* \approx 0.8329$ until the melting density at $\rho^* \approx 0.8897$ and remains same above the melting density.

3.2. Large SWCNTs

In this section the SWCNTs that can hold multi-layers of fluid particles are considered. The detailed parameters of the chosen SWCNTs are listed in Table 2. The equation of states for these SWCNTs is shown in Fig. 7. At the fluid-like branch we can observe that the pressure is higher for those SWCNTs of smaller diameters at the same density. The SWCNT (24, 0) shows the highest pressure and

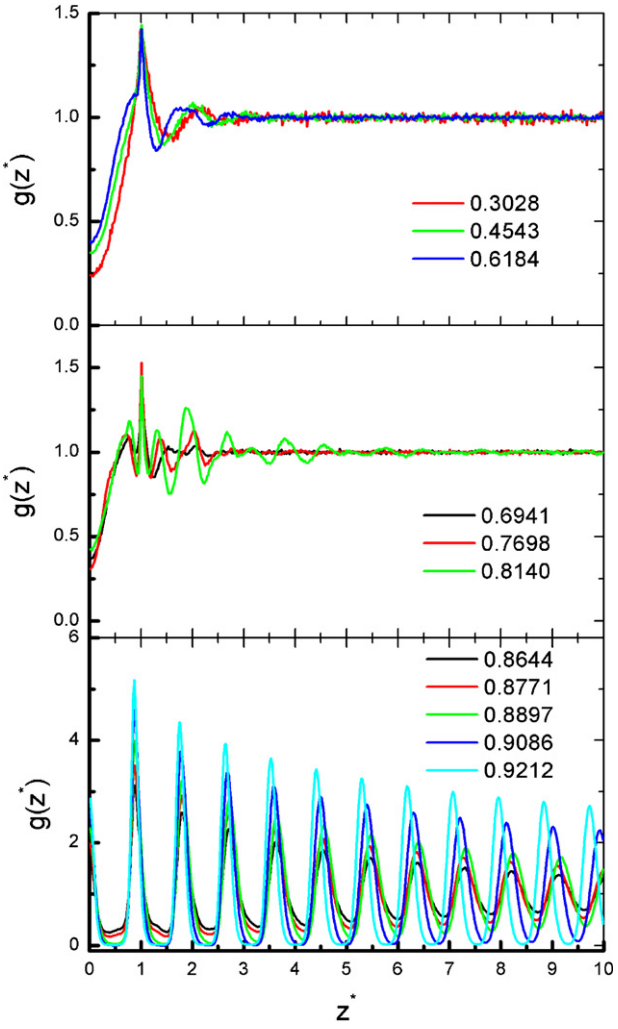

Fig. 5. Axial distribution function $g(z)$ of hard-spheres confined in SWCNT of chiral index (6, 5) at different densities from low (i.e. fluid-like) to high (i.e. solid-like).

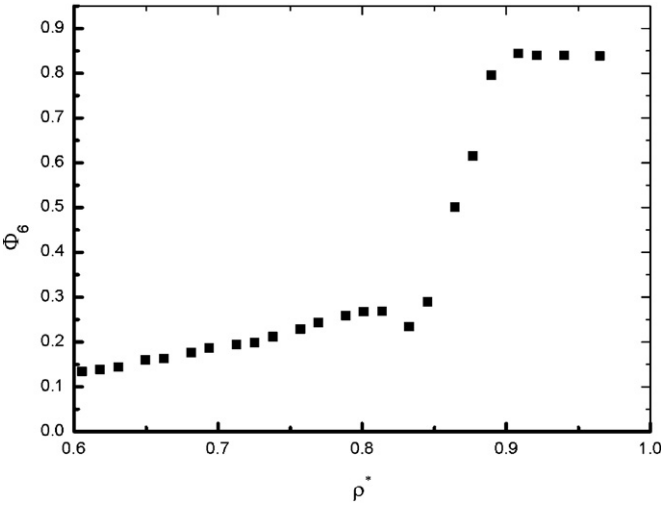

Fig. 6. Plot of the hexagonal order parameter Φ_6 vs. reduced density for hard-spheres confined in SWCNT of chiral index (6, 5). The sharp increase of Φ_6 shows the onset of freezing.

Table 2
Structure parameters for the large SWCNTs.[a]

Chiral index	Diameter ($2 \times r_t$)	Number of carbon atoms in unit cell	Length of unit cell	Number of unit cell	Length of SWCNT	Number of carbon atoms
(24, 0)	6.6845	96	1.5155	20	30.310888	1920
(14, 14)	6.7537	56	0.875	25	21.875	1400
(26, 2)	7.5355	488	6.8339	3	20.5019	1464
(16, 16)	7.7186	64	0.875	25	21.875	1600
(28, 0)	7.7985	112	1.5155	20	30.310888	2240
(20, 12)	7.7985	784	10.6088	2	21.2176	1568

[a] All length units are reduced by the diameter of hard-sphere fluid particle, σ_f.

the lowest pressure is found in the SWCNTs (28, 0) and (20, 12), which have the same diameter of 7.7985. The equations of states at the fluid-like branch almost overlap for those SWCNTs of close diameters. The most spreading pressures of (28, 0) and (20, 12) are overlapped, which indicates that the chiral difference of the SWCNTs of large diameters has less impact on the equation of states of the confined hard-sphere fluids. Compared to the small SWCNTs of chiral indices (6, 5) and (9, 1), which have identical diameters yet the freezing pressure of (9, 1) is larger than that of (6, 5).

The 2*D* hexagonal order parameters for the first and second layers of fluid particles for these SWCNTs are shown in Fig. 8. Both first and second layers of fluid particles are transformed from disordered structure to ordered hexagonal planes in the same manner. Such sharp change is considered associating with fluid-like to solid-like phase transition. From Fig. 8 it is interesting to observe that first (i.e. outer) and second (i.e. inner) layers show subtle differences for the onset of the freezing. From investigating Φ_6's in the case of (24, 0) and (14, 14), the outer layers start freezing first (i.e. smaller diameters), but freezing of both layers are indistinguishable when the diameters become larger. The freezing density of (14, 14) is found to be smallest (i.e. early onset of freezing) of all SWCNTs of interest, followed by the SWCNTs (24, 0) with slightly larger freezing density. The freezing and melting densities of (16, 16), (28, 0) and (20, 12) are much larger than those SWCNTs of (24, 0), (14, 14), and (26, 2). In general, the SWCNTs with larger diameter show larger freezing density of the confined fluids. Considering that the size of fluid particle is twice than that of carbon atom, different chirality is better taken into account when the phase behavior of the confined fluids is traced. This consideration must be done for the case of small diameter SWCNTs.

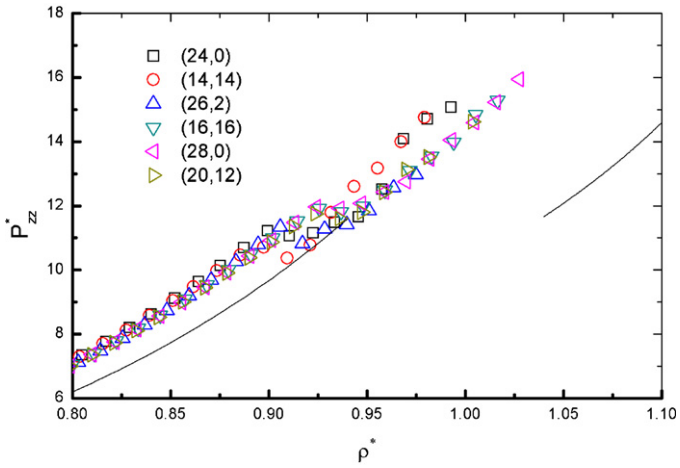

Fig. 7. The equation of states (i.e. reduced spreading pressure vs. reduced density) of hard-spheres confined in SWCNTs of different chiral indices, depicted by open symbols. In chiral index (n, m), the armchair-shaped SWCNT has same n and m values, and the zigzag-shaped SWCNT has zero for m. The line is for hard-sphere systems in bulk.

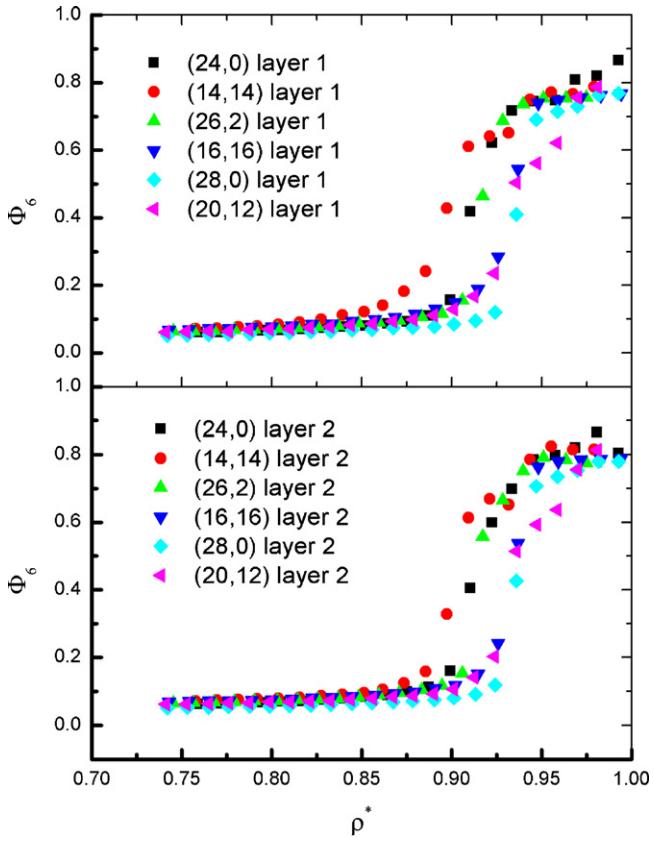

Fig. 8. Plot of the hexagonal order parameter Φ_6 for the first (i.e. contact layer with the SWCNT) and the second layer vs. reduced density for hard-spheres confined in SWCNTs of different chiral indices. In chiral index (n, m), the armchair-shaped SWCNT has same n and m values, and the zigzag-shaped SWCNT has zero for m.

4. Conclusion

In this work, we consider the hard-spheres confined by the particles following the configurations of the SWCNTs with different chiral indices. The fluid–fluid and fluid–carbon interactions are simplified as perfect elastic potentials and the carbon atoms are set to be stationary to capture intrinsic effects of the surface chirality on the confined particles. The fixation condition of carbon atoms is reasonable to imitate an expanded SWCNT, which has larger size of honeycombs than those in real SWCNT. In this way, the effect of the surface chirality would be more visible if any observed. The fluid particles can be self-assembled into layering structure driven by the help of the entropic driving-force. The chiral indices of the SWCNTs are chosen that the interior space of the SWCNTs can hold single or multiple layers of fluid particles. The equation of states of fluids confined in these SWCNTs are estimated and they show similarly three branches of fluid-like, coexistence, and solid-like. Clear junctions of the branches were able to be obtained via the 2D hexagonal order parameter. We find that in the small SWCNTs, the

structured walls of the SWCNTs dramatically induces early freezing at lower pressure and the difference of surface chirality has considerable impact on the freezing pressure while in large SWCNTs the impact is less observable. This is because, beside the fact that the size of fluid particle is twice big, we speculate that if the confined fluids have other layers by the contact layer, which is under the greatest effect from the surface chirality, the surface effect would be transferred from the outmost contact layer to inner layers so that the effect is offset. For those SWCNTs that contain only one layer of fluid particles, such impact is essential to the properties of the confined fluids.

Acknowledgments

This work was supported by Nanyang Technological University (NTU) under grant nos. M58120005/M52120043 and the computational resources have been provided by the school of chemical and biomedical engineering at NTU.

References

[1] L. Zhou, Y. Sun, Z. Yang, Y. Zhou, J. Colloid Interface Sci. 289 (2005) 347.
[2] Y. Zhou, K. Feng, Y. Sun, L. Zhou, Chem. Phys. Lett. 380 (2003) 526.
[3] A. Striolo, A.A. Chialvo, P.T. Cummings, K.E. Gubbins, J. Chem. Phys. 124 (2006) 074710.
[4] T. Belin, N. Millot, F. Villiéras, O. Bertrand, J.P. Bellat, J. Phys. Chem. B 108 (2004) 5333.
[5] J.K. Holt, H.G. Park, Y. Wang, M. Stadermann, A.B. Artyukhin, C.P. Grigoropoulos, A. Noy, O. Bakajin, Science 312 (2006) 1034.
[6] Y. Maniwa, K. Matsuda, H. Kyakuno, S. Ogasawara, T. Hibi, H. Kadowaki, S. Suzuki, Y. Achiba, H. Kataura, Nat. Mater. 6 (2007) 135.
[7] F. Mikami, K. Matsuda, H. Kataura, Y. Maniwa, ACS Nano 3 (2009) 1279.
[8] S. Iijima, Nature 354 (1991) 56.
[9] J. Sloan, J. Hammer, M. Zwiefka-Sibley, M.L.H. Green, Chem. Commun. 3 (1998) 347.
[10] B.W. Smith, M. Monthioux, D.E. Luzzi, Nature 396 (1998) 323.
[11] J. Sloan, D.M. Wright, H.G. Woo, S. Bailey, G. Brown, A.P.E. York, K.S. Coleman, J.L. Hutchison, M.L.H. Green, Chem. Commun. 8 (1999) 699.
[12] R.R. Meyer, J. Sloan, R.E. Dunin-Borkowski, A.I. Kirkland, M.C. Novotny, S.R. Bailey, J.L. Hutchison, M.L.H. Green, Science 289 (2000) 1324.
[13] J. Sloan, M.C. Novotny, S.R. Bailey, G. Brown, C. Xu, V.C. Williams, S. Friedrichs, E. Flahaut, R.L. Callender, A.P.E. York, K.S. Coleman, M.L.H. Green, R.E. Dunin-Borkowski, J.L. Hutchison, Chem. Phys. Lett. 329 (2000) 61.
[14] X. Fan, E.C. Dickey, P.C. Eklund, K.A. Williams, L. Grigorian, R. Buczko, S.T. Pantelides, S.J. Pennycook, Phys. Rev. Lett. 84 (2000) 4621.
[15] A. Kuznetsova, J.T. Yates, J. Liu, R.E. Smalley, J. Chem. Phys. 112 (2000) 9590.
[16] J. Mitta, M. Monthioux, H. Allouche, O. Stephan, Chem. Phys. Lett. 339 (2001) 311.
[17] B.W. Smith, D.E. Luzzi, Y. Achiba, Chem. Phys. Lett. 331 (2000) 137.
[18] K. Hirahara, K. Suenaga, S. Bandow, H. Kato, T. Okazaki, H. Shinohara, S. Iijima, Phys. Rev. Lett. 85 (2000) 5384.
[19] K. Suenaga, M. Tencé, C. Mory, C. Colliex, H. Kato, T. Okazaki, H. Shinohara, K. Hirahara, S. Bandow, S. Iijima, Science 290 (2000) 2280.
[20] J. Sloan, M. Terrones, S. Nufer, S. Friedrichs, S.R. Bailey, H.G. Woo, M. Rühle, J.L. Hutchison, M.L.H. Green, J. Am. Chem. Soc. 124 (2002) 2116.
[21] M. Hodak, L.A. Girifalco, Phys. Rev. E 67 (2003) 075419.
[22] P.M. Ajayan, C. Colliex, J.M. Lambert, P. Bernier, L. Barbedette, M. Tence, O. Stephan, Phys. Rev. Lett. 72 (1994) 1722.
[23] Y. Yosida, Appl. Phys. Lett. 64 (1994) 3048.
[24] F.R. Hung, B. Coasne, E.E. Santiso, K.E. Gubbins, F.R. Siperstein, M. Sliwinska-Bartkowiak, J. Chem. Phys. 122 (2005) 144706.
[25] M.W. Maddox, K.E. Gubbins, J. Chem. Phys. 107 (1997) 9659.
[26] M. Sliwinska-Bartkowiak, G. Dudziak, R. Sikorski, R. Gras, R. Radhakrishnan, K.E. Gubbins, J. Chem. Phys. 114 (2001) 950.
[27] M. Miyahara, K.E. Gubbins, J. Chem. Phys. 106 (1997) 2865.
[28] R. Radhakrishnan, K.E. Gubbins, M. Sliwinska-Bartkowiak, J. Chem. Phys. 116 (2002) 1147.
[29] F.R. Hung, G. Dudziak, M. Sliwinska-Bartkowiak, K.E. Gubbins, Mol. Phys. 102 (2004).
[30] M.C. Gordillo, B. Martínez-Haya, J.M. Romero-Enrique, J. Chem. Phys. 125 (2006) 144702.
[31] K.K. Mon, J.K. Percus, J. Chem. Phys. 112 (2000) 3457.
[32] F.J. Durán-Olivencia, M.C. Gordillo, Phys. Rev. E 79 (2009) 061111.
[33] G.T. Pickett, M. Gross, H. Okuyama, Phys. Rev. Lett. 85 (2000) 3652.
[34] H.C. Huang, S.K. Kwak, J.K. Singh, J. Chem. Phys. 130 (2009) 164511.
[35] K. Murata, K. Kaneko, W.A. Steele, F. Kokai, K. Takahashi, D. Kasuya, K. Hirahara, M. Yudasaka, S. Iijima, J. Phys. Chem. B 105 (2001) 10210.
[36] S. Agnihotri, J.P.B. Mota, M. Rostam-Abadi, M.J. Rood, Carbon 44 (2006) 2376.
[37] A. Fujiwara, K. Ishii, H. Suenatsu, H. Kataura, Y. Maniwa, S. Suzuki, Y. Achiba, Chem. Phys. Lett. 336 (2001) 205.
[38] H.C. Huang, W.W. Chen, J.K. Singh, S.K. Kwak, J. Chem. Phys. 132 (2010) 224504.
[39] J.M. Haile, Molecular Dynamics Simulation: Elementary Methods, Wiley-Interscience, 1997.